Video Article

Measuring Connectivity in the Primary Visual Pathway in Human Albinism Using Diffusion Tensor Imaging and Tractography

Anahit Grigorian[1], Larissa McKetton[1], Keith A. Schneider[1]

[1]Department of Biology, Centre for Vision Research, York University

Correspondence to: Anahit Grigorian at grig.annie@gmail.com

Abstract

In albinism, the number of ipsilaterally projecting retinal ganglion cells (RGCs) is significantly reduced. The retina and optic chiasm have been proposed as candidate sites for misrouting. Since a correlation between the number of lateral geniculate nucleus (LGN) relay neurons and LGN size has been shown, and based on previously reported reductions in LGN volumes in human albinism, we suggest that fiber projections from LGN to the primary visual cortex (V1) are also reduced. Studying structural differences in the visual system of albinism can improve the understanding of the mechanism of misrouting and subsequent clinical applications. Diffusion data and tractography are useful for mapping the OR (optic radiation). This manuscript describes two algorithms for OR reconstruction in order to compare brain connectivity in albinism and controls.An MRI scanner with a 32-channel head coil was used to acquire structural scans. A T1-weighted 3D-MPRAGE sequence with 1 mm^3 isotropic voxel size was used to generate high-resolution images for V1 segmentation. Multiple proton density (PD) weighted images were acquired coronally for right and left LGN localization. Diffusion tensor imaging (DTI) scans were acquired with 64 diffusion directions. Both deterministic and probabilistic tracking methods were run and compared, with LGN as the seed mask and V1 as the target mask. Though DTI provides relatively poor spatial resolution, and accurate delineation of OR may be challenging due to its low fiber density, tractography has been shown to be advantageous both in research and clinically. Tract based spatial statistics (TBSS) revealed areas of significantly reduced white matter integrity within the OR in patients with albinism compared to controls. Pairwise comparisons revealed a significant reduction in LGN to V1 connectivity in albinism compared to controls. Comparing both tracking algorithms revealed common findings, strengthening the reliability of the technique.

Video Link

The video component of this article can be found at https://www.jove.com/video/53759/

Introduction

Albinism is a genetic condition primarily characterized by overt hypopigmentation observed in affected individuals. It is caused by inherited mutations to genes involved in melanin synthesis[1]. Albinism appears in two main forms: oculo-cutaneous albinism (OCA), an autosomal recessive trait presenting both ocular and cutaneous features; and ocular albinism (OA), an X-linked trait more prevalent in males and characterized primarily by the ocular symptoms[2]. Melanin in the retinal pigment epithelium (RPE) is crucial for proper development of the central visual pathway. Its absence in albinism therefore results in visual impairments, including photophobia, nystagmus, reduced visual acuity and loss of binocular vision[2-3]. Visual acuity has been linked to foveal morphology, which is altered in albinism[4]. In humans, a retinal line of decussation lies along the nasotemporal border through the fovea, with fibers from nasal retina crossing to the other hemisphere and those from temporal retina extending ipsilaterally. The degree of reduced visual function in albinism has been linked to the level of hypopigmentation. Specifically, pigmentation is inversely proportional to the shift into temporal retina of the line of decussation[5]. As a result of the shift in line of decussation into the temporal retina, crossing of optic nerve fibers is increased – a characteristic common across all species[3].

Structural MRI studies on humans have shown narrower optic chiasms in albinism compared to controls, which is likely the result of increased crossing of RGCs observed in albinism[6-8]. The retina and optic chiasm express axonal guidance cues such as Eph family receptors and their ligands[9] and are therefore candidate sites for misrouting[10].

A study on monkeys with induced glaucoma revealed a significant decrease in the number of LGN parvalbumin-immunoreactive relay neurons and LGN volume[11]. This suggests a correlation between LGN size and the number of white matter (WM) trajectories traveling through the OR to V1. A post mortem study on human albinism also revealed smaller LGN with fused M and P layers[12]. High-resolution structural MRI confirmed significant reduction in volume of LGN in albinism[8]. Taken together, these findings suggest that decreased LGN volume may result in a reduced number of neurons in the LGN, and in turn in decreased connectivity between LGN and V1.

Examining patterns of anatomical connectivity in humans has been limited. Dissection, tracer injection and lesion induction are invasive techniques that can only be used post mortem, and usually involve a very small number of patients. Previous studies using carbocyanine dye DiI injections demonstrated neuronal connectivity between V1 and V2 (secondary visual cortex)[13], as well as within the hippocampal complex in aldehyde-fixed post-mortem human brains[14]. Labeling fibers in this way is restricted to distances of only tens of millimeters from the point of injection[14]. Diffusion tensor imaging, DTI, is an MRI modality developed in early-mid 1990s to identify fiber tract direction and organization. It is a non-invasive method that allows mapping of large WM pathways in the living brain. DTI is sensitive to the diffusion of water molecules in biological tissue[15]. In the brain, the diffusion of water is anisotropic (uneven) due to barriers such as membranes and myelin. WM has high diffusion anisotropy, meaning the diffusion is greater parallel to than perpendicular to the orientation of the fibers[16]. Fractional anisotropy (FA) is a scalar quantity that describes the preference of molecules to diffuse in an anisotropic manner. FA values range from 0-1, from low to high anisotropy (cerebrospinal fluid (CSF) <gray matter (GM) <WM)[16].

Streamline (deterministic) and probabilistic fiber tracking are two different algorithms for 3D path reconstruction. Deterministic tractography uses a line propagation method, connecting neighboring voxels in a defined seed region. Two stop criteria used in this algorithm are the turning angle and the FA value. Therefore, tract tracing between neighbouring voxels is unlikely at large turning angles. The algorithm would therefore also progresses only if the FA in a voxel exceeds a specific threshold, limiting its effectiveness in accurately defining pathways near gray matter, where anisotropy drops. Probabilistic tractography, on the other hand, yields a connectivity map describing the probability of a voxel to be part of a tract between two regions of interest (ROIs) and thus progresses into gray matter such as V1[17]. Using this MRI application, key WM structures like the OR can be delineated, as shown in previous studies[18-20].

This study therefore uses diffusion data and tractography to explore the effect of axonal misrouting on retino-geniculo-cortical connectivity. Based on previously reported reductions in LGN volumes in human albinism[8], we predict that fiber projections from LGN to V1 are also reduced (**Figure 1**).

Protocol

Ethics Statement: The current research study has been approved by the Human Participants Review Committee (HPRC) at York University, Toronto. All participants gave informed written consent.

1. Subject Preparation

Note: Eleven participants with OCA, aged 36 ± 4 years (6 females) were compared to ten age-matched controls, aged 32 ± 4 years (6 females). Participant history is recorded in **Table 1**.

1. Ask each participant to fill out and sign a consent form that lists MRI safety guidelines and imaging protocol.
2. For each participant, provide earplugs for the ears. Position participant supine and head first in the magnet, and landmark above the eyes at the eyebrow level. Secure participant's head with cushions to reduce head motion. Give the participant a squeeze bulb for patient alert.
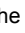
2. Structural MRI Parameters

Note: All imaging is acquired on a 3T MRI scanner using a 32-channel head coil. During a single session per subject:

1. Acquire a high resolution T1-weighted anatomical using a 3D-MPRAGE sequence covering the entire brain with the following parameters: acquisition time 4 min 26 sec, field of view 256 mm, 256 matrix, 192 slices with slice thickness of 1 mm, with a resulting isotropic voxel size of $1.0\ mm^3$, TR = 1900 ms, TE (echo time) = 2.52 ms with an inversion time of 900 ms and flip angle of 9°, 1 average, parallel imaging (iPat GRAPPA, acceleration factor of 2).
2. Acquire a DTI sequence covering the cortex, with slices in transverse orientation following the anterior commissure/posterior commissure (AC-PC) line, using the following parameters:acquisition time 8 min 5 sec, field of view 192 mm, 128 matrix, voxels 1.5 1.5 mm in-plane, 56 contiguous (no gap) slices with 2 mm thickness, TR = 6900 ms, TE = 86 ms, 64 directions, b-value of 1000 s/mm^2 (reference image with low b-value of 0 sec/mm^2), 1 average, parallel imaging (iPat GRAPPA) with an acceleration factor of 3.
3. Acquire 30-40 PD-weighted images in a coronal orientation, parallel to the brain stem,covering from the anterior extent of the pons to the posterior portion of the inferior colliculus.
   1. Use the Turbo spin echo (FAST spin echo) pulse sequence and the following parameters:acquisition time 1 min 29 sec per scan, field of view 192 mm, 256 matrix, 30-40 slices with thickness of 1 mm, resulting voxel size 0.75 0.75 1 mm^3, TR = 3,000 msec, TE = 22 msec, turbo factor of 5, refocusing flip angle of 120°, 1 average, parallel imaging (iPat GRAPPA) with an acceleration factor of 2. Note: S12 was scanned using the following parameters: field of view 180 mm, 512 matrix, 30 slices with 1 mm thick slices, resulting voxel size 0.4 x 0.4 x 1.0 mm^3. All other parameters remained the same. Acquisition time 2 min 47 sec.
4. Pre-process all scans by converting raw DICOM to NIfTI format using the program dcm2nii.

3. LGN Delineation

Note: The LGN is a small subcortical structure located deep in the brain, hence high-resolution PD images are required to determine its anatomical boundaries. In these scans, the LGN appears as an area of high signal intensity relative to the surrounding WM tracts, facilitating its detection[21]. The identified anatomical LGN is then used as a seed region for tractography.

1. While blind to group membership, manually trace right and left LGN masks three times each on averaged PD images interpolated to twice the resolution and half the voxel size (original 256 x 256 matrix, 0.75 x 0.75 x 1 mm^3 voxel size).

1. To obtain high resolution PD images use the freely available FLIRT function and other software tools within FMRIB's Software Library (FSL, http://www.fmrib.ox.ac.uk/fsl/). Upsample, concatenate, motion correct and average PD images for each participant as previously described elsewhere[22].
2. Load the high resolution PD image in FSLView and click on the Tools tab to select the Single option (or press ⌘) to enlarge the image.
3. Click the File tab to select the Create Mask option, and use the toolbar on the top left of the screen to trace the LGN in each slice. If desired, change the contrast of the image by dragging along the min/max in the toolbar to facilitate LGN detection.

2. Merge these regions of interest (ROIs) into a median mask using the fslmerge command.
3. Combine all raters' median masks into a single median mask using the same command.

4. V1 Segmentation

1. Run "recon-all" command in FreeSurfer23 (v5.3.0) on brains in native anatomical space (T1-weighted images) for automated processing.
2. Convert the appropriate outputs in the newly created mri folder (orig.mgz, brain.mgz, rawavg.mgz, T1.mgz) to NIfTI using "mri_convert".
3. Use BET brain extraction in the FSL GUI to correct the skull-stripped output brain (brain.nii.gz) in FreeSurfer space if necessary. Choose the Run standard brain extraction using bet2 option (default). Lower the threshold if image is missing brain tissue, or increase if non-brain tissue is captured (default threshold 0.5). Select the Output brain-extracted image and Output binary brain mask image (the latter may be used for manual corrections) in the advanced options.
4. Convert output V1 parcellation to a volumetric mask using "label2surf" and "surf2volume" commands.

5. Pre-tracking Registrations

Note: For the next steps, call the FSL GUI to open each of the following tools.

1. Use BET brain extraction and select the Bias field & neck cleanup option to skull-strip rawavg.nii.gz, located in the mri folder created by "recon-all". Adjust threshold as necessary.
2. Run FLIRT linear registration to bring brains in FreeSurfer and native anatomical space to diffusion space.
   1. Select brain.nii.gz, output of recon-all (FreeSurfer space), or a subject's brain extracted T1 (native anatomical space) as the input image, and an Eddy corrected and brain extracted diffusion-weighted image (DWI) as the reference image. Then click "Go".
   Note: This step creates two outputs, the input brain registered to the reference image (.nii.gz) and a transformation matrix (.mat). Apart from registration, the latter file is required for tractography when seed space is not diffusion. Use the output transformation matrices (.mat) created in this step for tractography as explained in 7.4.2.
3. Similar to 5.2, run FLIRT linear registration to bring participants' PD brains to FreeSurfer space and native anatomical space.
4. Prepare seed masks for tractography:
   1. Apply FLIRT transformation from Utils in the FLIRT linear registration toolbox. Use the .mat output as the transformation matrix, the original LGN mask as the input and brain.nii.gz (FreeSurfer space) or T1_brain.nii.gz (native anatomical space) (see 5.2) as the reference volume. Select the Nearest Neighbor interpolation method from the advanced options.
5. Using brain.nii.gz files only, prepare target masks for tractography:
   1. Register FreeSurfer brains to native anatomical space and create target masks by applying transformation to V1 masks (see 5.2, 5.4.1) using Tri-Linear interpolation. Click "Go".

6. LGN Normalization

1. Use FNIRT non-linear registration as described previously at http://fsl.fmrib.ox.ac.uk/fsl/fslwiki/FNIRT to bring participants' non-extracted brains in native anatomical space to MNI space, using the Montreal Neurological Institute whole brain template (MNI152).
   Note: Non-linear registration of original anatomical images is recommended for this step, as registrations were more accurate when FNIRT was applied to non-extracted T1s compared to FLIRT on extracted brains.
2. Apply transformation to LGN masks in anatomical space (original LGN previously transformed to native anatomical space in 5.4) using nearest-neighbour interpolation as described in 5.4.1 to bring masks to MNI space.
3. Average all LGN masks in MNI space across both groups using AFNI's "3dMean" command.
4. Use "fslmaths -thr" to apply a threshold to the mean mask in MNI space.
5. Calculate the radius of the mean mask in MNI space using $V = 4/3\pi r^3$ (assume a sphere).
6. Record the centre of mass coordinates of each individual LGN mask in native anatomical space using the command "fslstats -C".
7. Create spherical ROIs of identical volumes across participants:
   1. Use **"fslmaths"** to create an ROI point with the coordinates of the appropriate individual LGN mask in native anatomical space as recorded in 6.6
   2. Using "fslmaths", apply the radius of the mean mask in MNI space to create a sphere around the ROI point in native anatomical space.
8. Use these standardized masks as seeds for tractography.

7. Probabilistic Tractography (FSL 5.0.4)

Note: For the next steps, call the Fdt_gui to access each of the following tools.

1. Correct for distortions in DWIs with Eddy current correction. Select the Eddy current correction option from the menu at the top of the Diffusion Toolbox window and upload the DWI as the input, leaving the default reference volume (0).
2. Brain extract the images with BET as described in 4.3.
3. Select the DTIFIT Reconstruction diffusion tensors option from the menu. Specify an input directory containing the following files: diffusion weighted data, nodif_brain_mask (output of BET), bvec and bval (must be renamed to bvecs and bvals; text files containing information about diffusion image acquisition parameters, output of DICOM to NIfTI conversion of diffusion data). Click "Go" to run dtifit, which fits a diffusion tensor model at each voxel, creating files for post-processing.
4. Next, select the BedpostX (estimation of diffusion parameters) option from the menu. Use the same input directory as for DTIFIT. Click 'Go' to generate all files required for tractography.
5. From the same menu, choose ProbtrackX for probabilistic tracking and run it for each hemisphere separately. Keep default basic options (5,000 samples, 0.2 curvature and loopcheck applied) and select modified Euler for computing probabilistic streamlines from advanced options for increased accuracy.
   1. Select the output of BedpostX containing .merged files as the BEDPOSTX directory.
   2. Select single mask as seed space and load the transformed LGN mask (in native anatomical space) as the seed image, T1 (brain in native anatomical space) to diffusion transformation matrix as the seed to diffusion transform, and V1 (in native anatomical space) in "optional targets" (all but exclusion masks) as the target.
   3. Use default mesh convention (Caret) and load the brain in native anatomical space (T1 image) as the surface reference image.

6. Repeat ProbtrackX for probabilistic tracking using the standard spherical ROIs (created in step 6) as seed regions for tractography as described in 7.5.2. Upload ROIs in the same way transformed LGN (anatomical space) were uploaded in 7.5.2.
7. Re-run tractography (7.5), this time with seed (non-normalized) and target masks in FreeSurfer space with the addition of FreeSurfer's contralateral white matter border mask as an exclusion mask, to avoid any crossing over and ensure direct ipsilateral connections. Check the Surface option from the ProbtrackX toolbox and select FreeSurfer as mesh convention.
   Note: It is important to emphasize that tractography is always run from diffusion space, but Probtrackx for probabilistic tracking allows the input of seed and target masks in a different space, along with a transformation matrix to diffusion space. In this study, probabilistic tractography was run with masks in both native anatomical and FreeSurfer space (**Figure 2**).

8. Deterministic Tractography (DSI Studio)

1. Open Eddy corrected diffusion-weighted images in DSI Studio[24] by clicking on Step 1: Open Source Images. Load bvec and bval files onto a b-table window that is automatically opened to create a source (.src) file.
2. Load the generated Source files onto the reconstruction window to modify the default reconstructed brain masks as necessary.
3. Then, select DTI as the reconstruction method[25] and run it on the source files to produce fiber information files (.fib).
4. Bring Participants' PD brains to diffusion space using FLIRT linear registration.
5. Apply transformation to LGN masks using nearest neighbor interpolation as described in 5.4.1.
6. Open .fib files in the program's tracking window.
7. Run tracking for each hemisphere separately, using LGN in diffusion space as the seed and Region 17 (V1) from Brodmann atlas available from DSI Studio as the terminative region. Load the LGN mask by clicking the Regions tab and Open Region. Select the Seed option under Type in the Region List on the left of the screen. To load the V1 mask from the atlas, click on Atlas from the toolbar in the Region List and select the appropriate atlas.
8. In each run, set the contralateral WM (named left/right-cerebral-white-matter) mask from FreeSurfer segmentation atlas (see Region List box in the tracking window) as a region of avoidance (ROA).
9. Repeat tracking (8.7-8.8) using spherical ROIs in diffusion space instead of individual LGN as seed regions for tractography.
   Note: The spherical ROIs have the same volume across all subjects and are centered on the center of mass of each LGN.
10. Repeat LGN normalization, section 6, only this time registering brains in diffusion space to standard MNI space, and applying transformations to LGN in diffusion space (original LGN previously transformed to diffusion space in 8.4-8.5) to bring masks to standard MNI space. Calculate the volume of the spherical ROI as the mean volume of all LGN across subjects in MNI space.
    Note: Tracking parameters can be modified by the user. For most runs, default tracking parameters were applied. For some individuals (A5, A7, S12), anisotropy threshold (default 0.14-0.15) was lowered (0.10-0.12) and angular threshold (default 60) was increased (65-85) for nicer visualization. A schematic of the technique is shown in **Figure 3**.

9. Statistical Analysis – TBSS (FSL)

Note: Tract-based spatial statistics is a voxelwise statistical analysis of participants' FA maps16 obtained with dtifit26. It is extensively used for statistics on diffusion data. This voxelwise approach overcomes potential alignment and smoothing problems seen in VBM-style FA analysis and provides whole brain investigation, unattainable through tractography-based approaches16.

1. Run "tbss_1_preproc" on the FA data located in a newly created TBSS directory.
2. Run "tbss_2_reg" – T to apply non-linear registration, bringing each participant's FA data into common space (FMRIB58_FA, target image in TBSS).
3. Create a mean FA skeleton with the centers of all common tracts among participants using **"tbss_3_postreg -S"**.
4. Run "tbss_4_prestats 0.2" to project each participant's aligned FA map onto the mean skeleton of all aligned FA maps.
5. Create design.con and design.mat files, ensuring that the order of the matrix is consistent with the order in which TBSS pre-processed the FA data.
6. Run "randomise", using the T2 option, which is recommended for TBSS as it acts on a skeleton (a reduced subset of the 3D data), and 5,000 pre-mutations, which gives more accurate p-values.

10. Statistical Analysis – SPSS

1. Extracting FA Values from Deterministic Data
   Note: Deterministic-based FA values were derived from DSI Studio output statistics text files. These values represent the mean FA within the generated tracts, which in this case correspond to the region of the OR.
   1. Run fiber tracking in DSI studio.
   2. Save the 'statistics' text files created by DSI Studio for each generated set of tracts and record the 'FA mean' values from them.

2. Extracting FA Values from Probabilistic Data
   Note: Probabilistic-based FA values are derived from ProbtrackX2 output fdt_paths files. These are 3D tract density images that in this study cover the area corresponding to the OR.
   1. Use FLIRT linear registration to bring each participant's fdt_paths files to diffusion space.
   2. Binarize the output masks using "fslmaths - bin".
   3. For each participant, multiply the mask by their FA map from dtifit using "fslmaths -mul".
   4. Run "fslmeants" command to find the mean FA from each tract mask.

3. Running Analyses with SPSS (Using Deterministic and Probabilistic Data)
   Note: Statistical analysis is performed using SPSS 20 for Mac. Since hemisphere is a within-subject variable, a generalized linear model (GENLIN) with which the effects in each side of the brain can be looked at separately, is applied. Specifically, the generalized estimating equation (GEE) is used.
   1. In separate tests, set each of mean FA and streamline count (waytotal or percentage generated streamlines, PGSL) as the dependent variable.
      Note: In this study, streamline count is based on way-total values. Waytotal describes the total number of generated streamlines that have not been rejected by inclusion/exclusion criteria[27]. The number of generated streamlines (NGSL), which refers to the total number of streamlines sent, is equal to the number of voxels in the seed mask multiplied by the number of samples drawn from each voxel (5,000 in this case). Percentage generated streamlines (PGSL), waytotal divided by NGSL times 100, is a measure of successful connectivity between the seed and the target.
   2. Study the influence of group and gender on LGN to V1 connectivity by setting them as independent variables in all tests.
      Note: Main effects as well as two- and three-way interactions were studied. It is important to note that these individual tests are not conditioned to each other, so the significance of one main effect or interaction is independent of the other.
   3. Use age as a covariate for all tests. Also, use LGN volume as a covariate for tests with mean FA and waytotal as the dependent variables, but omit it from tests with PGSL as the dependent variable.
      Note: Total brain volume was found to be an insignificant covariate and was therefore omitted from stats.
   4. Select the Bonferroni correction method to adjust for multiple comparisons[28] (level of significance p <0.05).

Representative Results

This section provides a summary of results obtained using two different algorithms of tractography, deterministic and probabilistic. LGN volumes in PD space in which masks were originally drawn, as well as in all other spaces used in this study, are recorded in **Table 2**, and LGN tracing is illustrated in **Figure 4**. The results reported here are based on runs that used a standard sphere as the LGN ROI. Standard LGN volume was 461 mm^3 in both hemispheres in anatomical space (probabilistic run), and 292.5 mm^3 and 364.5 mm^3 in the right and left hemispheres, respectively, in diffusion space (deterministic run). For both runs, these standard volumes are very close to the mean volumes calculated in MNI space (anatomical to MNI: 472 mm^3 and 440 mm^3 for left and right, respectively; diffusion to MNI: 376 and 312 mm^3 for left and right, respectively) but larger than most individual LGN volumes in native space (largest in anatomical: 281 mm^3; largest in diffusion: 324 mm^3). Since Bonferroni is a very conservative test, p values smaller than 0.1 are treated as approaching significance and are reported here. Additionally, TBSS on FA maps revealed areas of significant difference (p <0.05) between the two groups, with areas in red representing regions of reduced white matter tract integrity in albinism (**Figure 5**).

For both deterministic and probabilistic runs, covariates and three way group by gender by hemisphere interactions were insignificant and therefore excluded from all final analyses. For the deterministic run, using mean FA as the dependent variable, main effects of group and gender were insignificant, while the main effect of hemisphere approached significance (means ± SEM .41 ± .008 right; .39 ± .006 left, p = .064). Means (± SEM) of mean FA values corresponding to the OR region connecting LGN to V1 were 0.39 ± 0.007 for albinism and 0.40 ± 0.008 for controls. A two-way interaction of group by hemisphere was significant (p = .013). For the probabilistic run, using mean FA values from fdt_paths as the dependent variable, the main effect of group was insignificant (mean ± SEM .353 ± .0035 controls; .349 ± .0046 albinism). However, the main effects of hemisphere (.358 ± .004 right; .345 ± .003 left, p = .005) and gender (.34 ± .004 females; .36 ± .004 males, p = .014) were significant. A two way group by gender interaction was significant (p = .033). Data for all tests were normally distributed as confirmed by the Shapiro-Wilk test (p >0.05). Using the deterministic approach, mean waytotal values were 2,728 ± 127 for albinism and 2,753 ± 169 for controls. The main effect of hemisphere and the two way group by gender interaction were significant (p = .027 and p = .004, respectively). Using PGSL as the dependent variable, the main effects of group and gender were insignificant, while the effect of hemisphere was significant (means ± SEM 0.89 ± .045 right; 0.63 ± .026, p = .001). The two way group by gender interaction was also significant (p = .003). Mean PGSL from LGN to V1 were 0.76 ± .046 for albinism and 0.76 ± .048 for controls. PGSL were calculated using standard LGN ROI. Data were normally distributed (Shapiro p >0.05). For the probabilistic run, using waytotal values and PGSL as dependent variables, the main effects of group, hemisphere and gender were not significant. Mean waytotal values were 28,739 ± 7,297 for albinism and 31,220 ± 7,202 for controls. Mean PGSL from LGN to V1 were 1.3 ± .3 for albinism and 1.4 ± .3 for controls. In both cases, data were non-normally distributed and gamma log transformation was applied.

Using the deterministic approach, pairwise comparisons revealed reduced FA in the right hemisphere of albinism compared to controls (C^2(1, N = 21) = 4.15, p = .042). In controls, the left hemisphere FA value was lower than that for the right hemisphere (p =.007), and a trend for decreased FA in females compared to males was found (C^2(1, N = 21) = 2.97, p =.085). Using probabilistic tractography, pairwise comparisons revealed reduced FA in the left hemisphere compared to the right hemisphere in both groups (C^2(1, N = 21) = 6.31, p = .012). In males, FA was significantly reduced in albinism compared to controls (C^2(1, N = 21) = 4.27, p = .039). Also, FA was significantly decreased in females compared to males in controls (C^2(1, N = 21) = 14.37, p <0.001). Using waytotal values from the deterministic run as the dependent variable, pairwise comparisons revealed reduced connectivity in males with albinism compared to male controls (C^2(1, N = 21) = 4.65, p = .031). In both groups, connectivity in the left hemisphere was lower compared to the right hemisphere (C^2(1, N = 21) = 4.34, p = .037). Additionally, connectivity was lower in males compared to females in the albinism group (C^2(1, N = 21) = 4.47, p = .034), while the opposite was seen in the control group (C^2(1, N = 21) = 3.87, p = .049). Lastly, in females, a trend for decreased connectivity was seen in controls compared to albinism (C^2(1, N = 21) = 3.52, p = .061). Using PGSL values calculated from deterministic data, pairwise comparisons revealed similar results to those obtained with waytotal values. Outputs of deterministic tractography are illustrated in **Figure 6**. Using probabilistic data, pairwise comparisons revealed decreased connectivity in the right hemisphere of males compared to females (C^2(1, N = 21) = 15.96, p <0.001). Outputs of probabilistic tractography are illustrated in **Figure 7**. A Pearson's correlation revealed a very weak negative correlation between PGSL values from both methods (r = -0.172, p = 0.276; however, the fiber tracts largely overlap and are qualitatively similar (**Figure 8**).
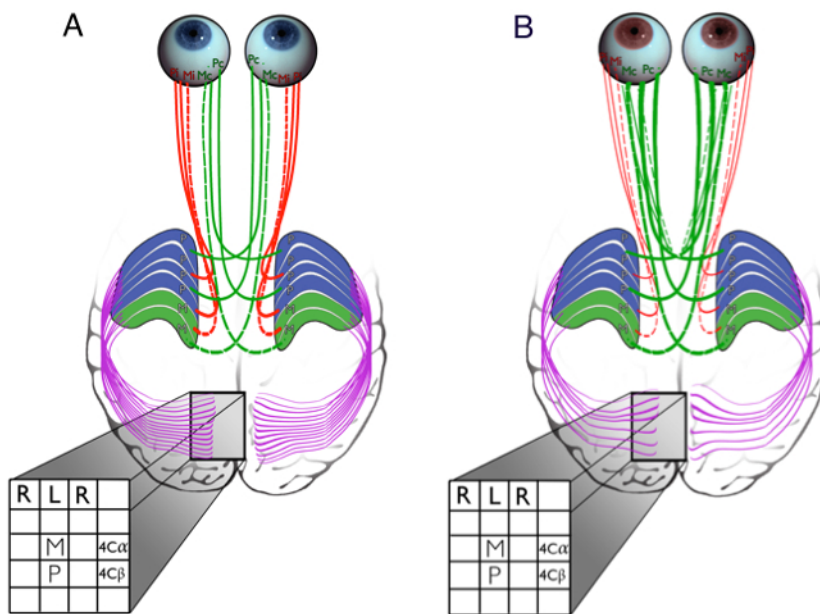

Figure 1: Primary Visual Pathway in the Brains of Healthy Individuals and Patients with Albinism. Each LGN receives inputs from both eyes. Ipsilateral retinal projections terminate on Layers 2, 3 and 5, while contralateral projections end on Layers 1, 4 and 6. The LGN sends projections to V1 via the optic radiation (purple), with axons terminating most heavily on V1 Layer 4. Inputs from the two eyes remain segregated in the ocular dominance columns of Layer 4. Beyond this point, inputs from both eyes are combined (binocular neurons in the cortex). (**A**) In controls, roughly half of the projections extend ipsilaterally (red) from the temporal retina, while the other half arise from the nasal retina and cross (green) at the chiasm to the contralateral hemisphere. (**B**) In albinism, there is a shift in line of decussation into the temporal retina, resulting in increased crossing of optic nerve fibers, as illustrated by the thickened green fibers. This schematic suggests additional abnormalities further downstream the retino-geniculo-cortical pathway, with reduced LGN to V1 connectivity in albinism (modified from Mcketton *et al.*, 2014) as confirmed by this study. Please click here to view a larger version of this figure.
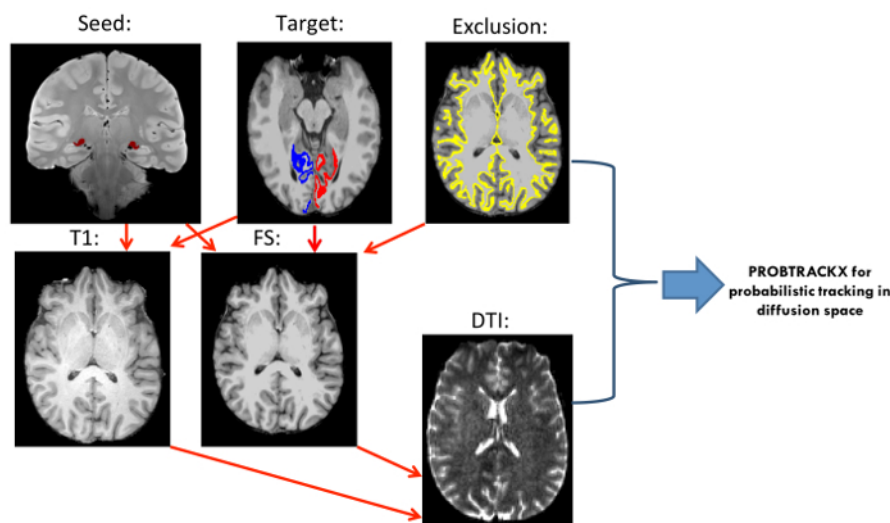
Figure 2" Probabilistic Tractography Pipeline. FLIRT Linear Registration was used to Transform Participants' Brains to Different Spaces (registration indicated by red arrows): In preparation of seed masks, PD brains were registered to anatomical T1 space and to FreeSurfer (FS) space, and transformations were applied to original LGN masks using nearest-neighbor interpolation. To create the target masks, FS brains were transformed to T1 space and transformations were applied to FreeSurfer's V1 masks using tri-linear interpolation. T1 and FS brains were linearly registered to diffusion space. FreeSurfer's contralateral white matter border mask was added as exclusion mask in the FS run. PROBTRACKX2 for probabilistic tracking was run in diffusion space with masks input in T1 and FS space. Please click here to view a larger version of this figure.
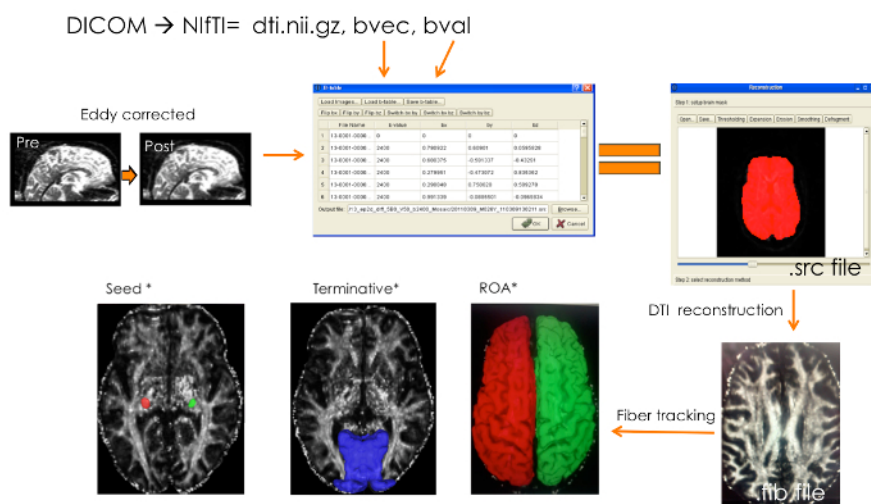

Figure 3: Deterministic Tractography Pipeline. Pre-processing Involved DICOM to NIfTI Conversion and Yielded a Diffusion-Weighted Image (dti.nii.gz) along with Two Text Files (bvec and bval). Distortions and movement were corrected for using FSL's Eddy-current correction tool. Eddy corrected diffusion-weighted images were opened in DSI Studio and bvec and bval files were loaded onto a b-table window to create a source (.src) file. Source files were opened and the default reconstructed brain masks were modified as necessary. Next, DTI reconstruction model was applied to the source files to produce fiber information files (.fib). LGN masks in diffusion space were loaded onto the .fib files in the tracking window and set as seeds. Region 17 (V1) from Brodmann atlas was set as a terminative region. In each run, the contralateral WM mask from FreeSurfer segmentation atlas was loaded and set as an ROA (both hemispheres delineated here). Equal signs represent the product yielded in a particular step; Orange arrows indicate the input file that was used for the next processing or tracking step; Asterisk (*) denotes masks and brains in diffusion space. Please click here to view a larger version of this figure.
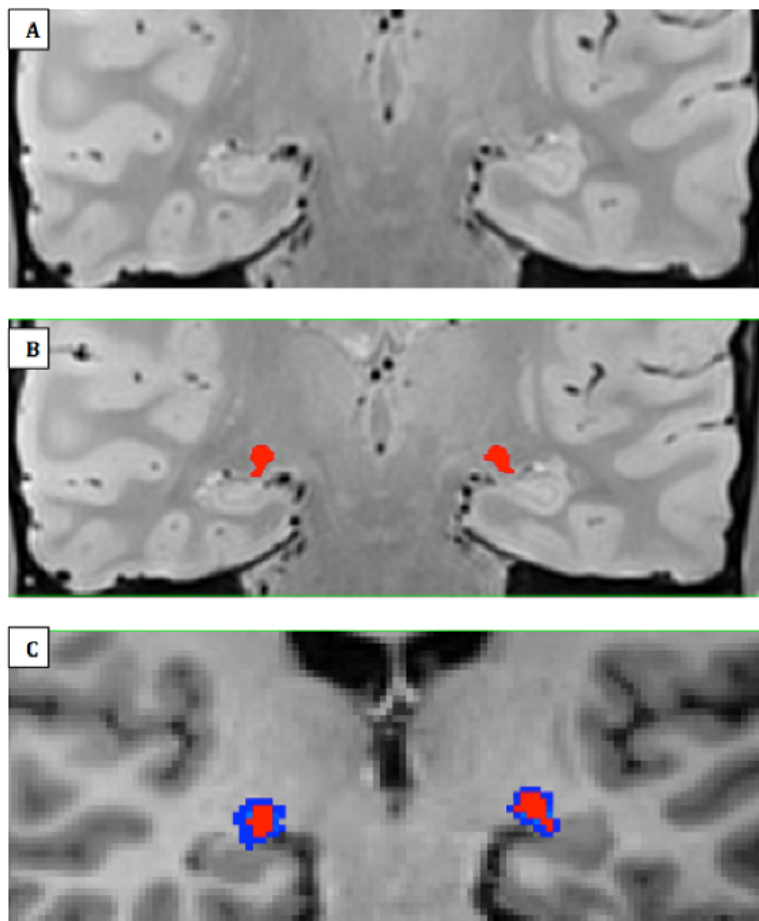
Figure 4: LGN Mask Delineation. (**A**) Zoomed-in view of right and left LGN on an averaged coronal PD-weighted image slab that was interpolated to twice the resolution and half the voxel size in a patient with albinism, A11. (**B**) Manually traced right and left LGN areas of interest (ROIs) in red (**C**) LGN masks transformed to FreeSurfer space using nearest neighbor (red) and tri-linear (blue) interpolations. The former was used for all transformations performed in this study for more accurate delineation of the structure. Please click here to view a larger version of this figure.

Figure 5: Voxelwise Statistical Analysis with TBSS. Whole brain voxelwise statistical analysis of FA data was carried out using tract-based spatial statistics (TBSS). Non-linear registration of all participants' FA images to a common space was performed, followed by the creation of a mean FA skeleton and the projection of each participant's FA image onto the skeleton. (**A**) Albinism > control contrast showing skeleton in green with no areas of significance due to reduced FA in albinism compared to controls. (**B**) Significant difference between the control group and the albinism group detected, with areas in red representing regions (cerebral white matter corresponding to optic radiation fibers and calcarine cortex, on which they terminate) of reduced white matter tract integrity in albinism, for the control>albinism contrast (TFCE (threshold-free cluster enhancement) corrected, *p* <0.05), (**C**) Thickened skeletonised version of results displayed in B, for visual representation. Please click here to view a larger version of this figure.
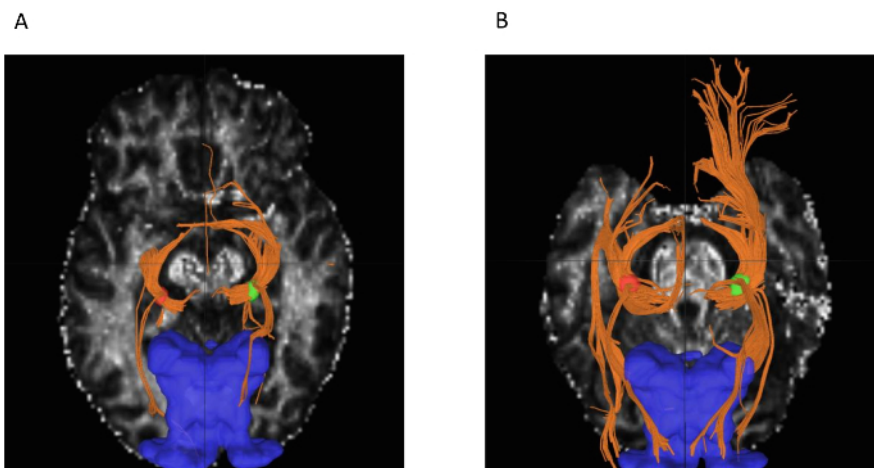
Figure 6: Output of DSI Studio Fiber Tracking. (**A**) Reduced LGN to V1 connectivity in albinism patient A1 (lowest number of reconstructed tracts among participants in right hemisphere, 1365) compared to (**B**) controls (S6, highest number of reconstructed tracts among controls in right hemisphere, 4355) (left LGN in red, right LGN in green, LGN connections to optic tract and OR in orange, V1 in blue). Optic tract to LGN connections are also seen in the output. Please click here to view a larger version of this figure.

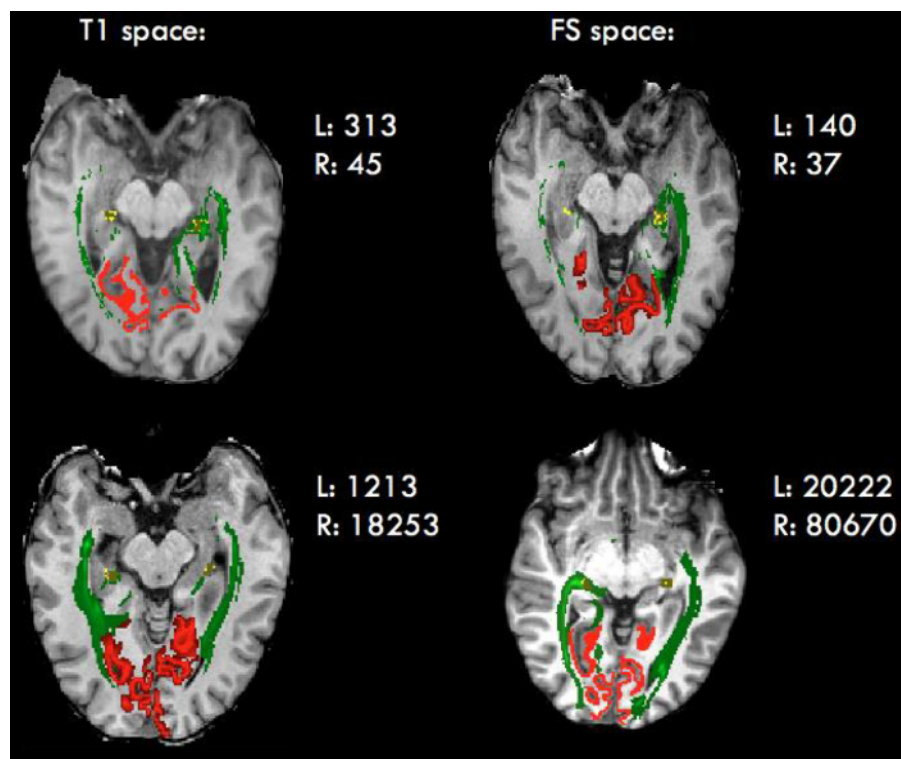**Figure 7: Output of PROBTRACKX for Probabilistic Tracking.** Reduced LGN to V1 connectivity in albinism (top) compared to controls (bottom). LGN is shown in yellow, optic radiation in green, V1 in red. Note that the slices shown here are not intended to be the same, but are rather chosen as slices that best represent the findings of the method. Please click here to view a larger version of this figure.
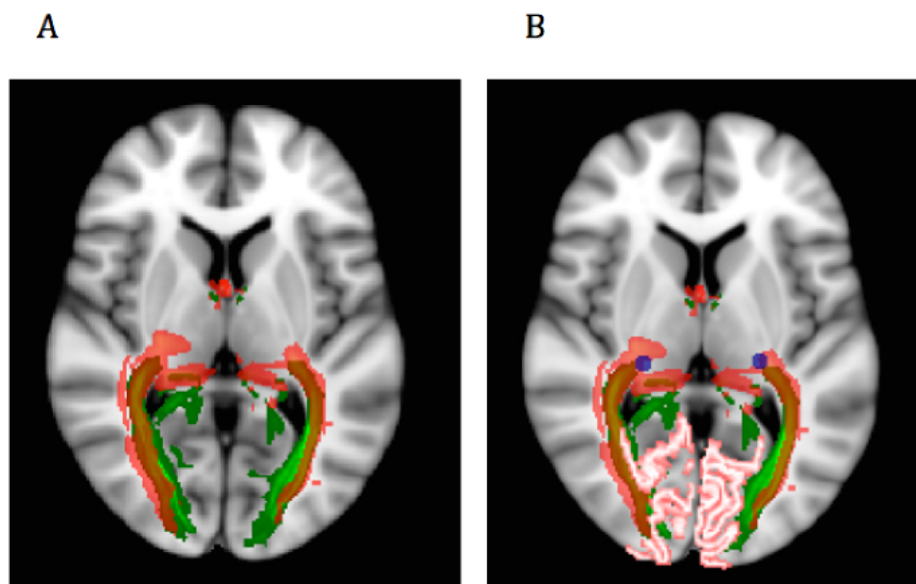
A

B

Figure 8: Probabilistic *versus* Deterministic Output Overlap Map. Anatomical brains (probabilistic run) and diffusion brains (deterministic run) were registered to 1mm MNI brains. Transformations were applied to tractography output tracts from runs that used standard spheres as LGN ROI. Output tracts were averaged across participants in each method, and (**A**) mean tract masks were overlaid on a 1 mm MNI brain in FSL view for comparison (probabilistic in green, deterministic in red). Transparency was applied to depict similar notions of connectivity in both methods. (**B**) LGN (blue) and V1 (pink) masks were added to illustrate the seed and target regions. Please click here to view a larger version of this figure.

Albinism					Controls		
Participant	**Age (yr)**	**Sex**	**Classification**	**Visual Acuity**	**Participant**	**Age (yr)**	**Sex**
A1	48	M	OCA	0.6	S1	24	F
A2	20	M	OCA-1	0.8	S2	22	M
A3	21	M	OCA-1A	1.0	S3	25	M
A4	48	M	OCA-1	1.0	S4	24	F
A5	43	F	OCA-1	0.8	S5	20	F
A6	56	M	OCA	0.9	S6	39	M
A7	22	F	OCA	0.6	S7	26	F
A8	47	F	OCA	0.9	S8	42	F
A9	45	F	OCA	1.0	S9	41	F
A10	17	F	OCA-1	0.9	S10	60	M
A11	29	F	OCA-2	0.5			

Table 1: Participant Information and Health History. Visual acuity was assessed using an Early Treatment Diabetic Retinopathy Study (ETDRS) eye chart and expressed in LogMar (logarithm of the minimum angle of resolution) notation, that is, the logarithm to the base 10 of decimal visual acuity (0.0-1.0 for 20/20-20/200). ETDRS chart testing has been shown to be more accurate than the universally used Snellen test[29]. All controls had normal or corrected-to-normal visual acuity (20/20). No history of neurological disorders was reported.

		PD		Anatomical		Diffusion		FS	
		Left	Right	Left	Right	Left	Right	Left	Right
Albinism	A1	48	71	57	78	63	72	49	67
	A2	195	176	199	179	194	162	212	190
	A3	191	181	203	186	180	171	194	184
	A4	119	99	132	110	122	122	129	113
	A5	128	132	101	106	153	113	135	153
	A6	128	75	75	75	86	104	84	85
	A7	115	105	101	95	117	113	117	114
	A8	63	49	54	56	45	32	79	40
	A9	81	105	81	104	77	113	76	112
	A10	120	122	115	117	131	126	156	156
	A11	69	92	70	93	81	113	75	98
Controls	S1	201	234	217	240	198	297	205	250
	S2	158	165	126	131	180	135	112	115
	S3	172	184	204	212	167	180	186	199
	S4	153	119	140	112	162	167	166	121
	S5	276	229	281	247	324	239	292	243
	S6	187	202	203	230	149	176	191	193
	S7	242	250	199	209	270	239	206	235
	S8	196	112	213	125	194	104	209	136
	S9	212	236	224	256	225	234	224	256
	S10	193	151	190	152	212	176	211	158

Table 2: A Summary of LGN Volumes. The volumes recorded in this table (mm³) are of right and left LGN of patients and controls in all spaces used in this study.

Discussion

Altered WM and, more specifically, decreased connectivity in albinism compared to controls were expected. Thus, the reduced FA in the right hemisphere of albinism compared to controls as well as the decreased connectivity in male patients with albinism reported here are in line with our prediction. Gender and hemisphere effects are not completely clear, although research on the healthy brain that suggests decreased WM complexity in the left hemisphere of males compared to females[30-31] could explain some of the gender- and hemisphere-related differences observed in this study. Reduced connectivity in male albinism compared to female albinism may be in part due to the younger average age of females in both groups (7-8 years < males), as WM volume was reported to be decreased in mid-adulthood in the healthy brain[32-33]. Gender differences may also be due to the small sample size and the uneven number of males versus females in each group (5 males OCA, 4 controls). The increased connectivity observed in female albinism compared to controls of the same gender was not expected, and might suggest some sort of a compensatory mechanism in albinism. However, this finding could rather be attributed to the great variability within a small population sample.

Mean FA and streamline count are used to explore LGN to V1 connectivity. FA is one of the most commonly reported measures derived from diffusion data. It is most accurately described as a quantification of how strongly directional diffusion is in a region. It is important to note that group differences in FA measures do not necessarily imply differences in white matter integrity. Since this study involves a clinical condition with a potential effect on white matter, such interpretation can be justified. However, while reduced integrity suggests structural damage or decline, FA in a region may be lowered due to fewer barriers such as larger axon diameters and less densely packed axons, as well as due to less effective boundaries resulting from increased membrane permeability[34]. The term 'streamline count', is preferred over 'fiber count', since the number of reconstructed streamlines may not be a true representation of the number of actual fibers due to variations in pathway features such as length, curvature and branching, as well as experimental conditions such as signal-to-noise ratio (SNR)[34].

Tractography is the only non-invasive technique for mapping WM *in vivo*. In the deterministic approach, termination occurs when anisotropy drops below a certain level, or when there is an abrupt angulation. However, most voxels contain fibers in more than one direction, and the deterministic approach is limited to either identifying the dominant tract in a voxel or an "average" of all directions within a voxel. It thus fails to provide a true representation of neuronal pathways. Probabilistic tractography allows the resolution of two fiber models in a single voxel, providing a more reliable representation of a tract, and tracking in areas of low anisotropy[17]. The probabilistic algorithm was therefore particularly advantageous in this study, which investigated the trajectory of the OR, a highly branching WM structure (particularly the portion of Meyer's loop), terminating in the gray matter of V1. It is important to note that probabilistic tractography refers to a stochastic probability of having the same pathway emerge over multiple permutations, rather than the misleading notion of tractography representing the true anatomy of a fiber.

Although probabilistic tractography is believed to follow the true course of nerve fibers more closely, deterministic tractography was run to compare the usefulness and reproducibility of both techniques. Since trends were detected using the probabilistic approach, similarities seen in the deterministic run only further strengthened the validity of the results.

Apart from its increasing use in research on mapping anatomical connectivity in the brain, tractography has shown promising advances in neurosurgical panning. Visualization of OR during resection of tumours by neuronavigationally transferring DWI data into the operative field was reported to help in successfully removing lesions and keeping the visual fields intact[35]. Nevertheless, DTI has limitations such as relatively poor spatial resolution and impaired data quality when structures with low fiber density such as the OR are studied[20]. Though probabilistic tractography was the preferred technique, the current study aimed to compare the two algorithms. Both tracking algorithms revealed some common findings, increasing the reliability of the results.

LGN volume ranges from 112-276 mm^3 in healthy brains[8] and correlates with volumes of the visual cortex and the optic tract, but not with overall brain volume[36]. Since tractography depends on the number of voxels in the seed mask, LGN volume should be normalized across participants to prevent bias in quantitative comparisons between tracts[37]. We controlled for differences in LGN size using two different methods. In the first method, spherical ROIs of a standard size were created. To achieve this, a mean volume across all subjects of their LGN masks transformed into MNI space was calculated. Using the radius of the mean mask in MNI space, a sphere was centered on the center of mass of each LGN in either anatomical or diffusion space. Using a standard sphere ROI with a volume larger than the individual LGN volumes ensures the inclusion of all voxels that are part of this structure in all participants. While using a larger mask size would usually increase the risk for false positives, such concern does not apply when seeding in a structure such as the LGN, which differs in connectivity patterns from surrounding nuclei. Hence, voxels belonging to other structures will generate streamlines that do not follow the expected paths and such paths will therefore be discarded[18]. The second method we used to control for LGN volume was to run statistical analyses using LGN volume as a covariate, but this did not significantly alter the statistical results. Another possible approach for LGN normalization is the addition and removal of voxels around individual LGN masks to obtain a standard size across subjects using a MATLAB script. This approach does not require any additional registrations and therefore limits the degree of deformation of the brain images and increases accuracy. It also retains the LGN outline rather than creating a sphere around the LGN region. However, to minimize human error, multi-atlas segmentation may be used instead of manually tracing the LGN masks. Using a set of atlases accounts for individual structural variability and therefore yields a more accurate representation of a subcortical region than a single atlas[38].

This novel *in vivo* study investigates interdependent development among different parts of the primary visual pathway in human albinism. It thus provides further insight into the etiology of this condition and improved diagnosis through identification of disorder-specific signatures. Both probabilistic and deterministic tractography algorithms used here showed comparable patterns of altered LGN to V1 connectivity in human albinism. Though no generalization to the large population can be made due to the small sample size and the large inter-subject variation in structures of interest, this study demonstrates the usefulness of tractography in detecting trends within the sample population, suggesting the importance of further research in the field.

Disclosures

The authors declare no conflict of interest.

Acknowledgements

References

1. Montoliu, L. *et al.* Increasing the complexity: new genes and new types of albinism. *Pigment Cell Melanoma Res.* **27**, 11-18 (2013).
2. Martinez-Garcia, M., & Montoliu, L. Albinism in Europe. *J. Dermatol.* **40** (5), 319-324 (2013).
3. Gottlob, I. Albinism: a model of adaptation of the brain in congenital visual disorders. *Br. J. Opthalmol.* **91** (4), 411-412 (2007).
4. Wilk, M.A., *et al.* Relationship between foveal cone specialization and pit morphology in albinism. *Invest. Ophthalmol. Vis. Sci.* **55** (7), 4186-4198 (2014).
5. Von dem Hagen, E.A.H., Houston, G.C., Hoffman, M.B., Morland, A.B. Pigmentation predicts the shift in the line of decussation in humans with albinism. *Eur. J. Neurosci.* **25**: 503- 511 (2007).
6. Rice, D.S., Williams, R.W., & Goldowitz, D. Genetic control of retinal projections in inbred strains of albino mice. *J comp neurol.* **354** (3), 459-469 (1995).
7. Schmitz, B., Schaefer, T., Krick, C.M., Reith, W., Backens, M., & Kasmann-Kellner, B. Configuration of the optic chiasm in humans with albinism as revealed by magnetic resonance imaging. *Invest. Ophthalmol. Vis. Sci.* **44** (1), 16-21 (2003).
8. Mcketton, L., Kelly, K.R., Schneider, K.A. Abnormal lateral geniculate nucleus and optic chiasm in human albinism. *J. Comp. Neurol.* **522** (11), 2680-2687 (2014).
9. Williams, S.E. *et al.* Ephrin-B2 and EphB1 mediate retinal axon divergence at the optic chiasm. *Neuron.* **39** (6), 919-935 (2003).
10. van Genderen, M.M., Riemslag, F.C., Schuil, J., Hoeben, F.P., Stilma, J.S., & Meire, F.M. Chiasmal misrouting and foveal hypoplasia without albinism. *J. Opthalmol.* **90** (9), 1098-1102 (2006).
11. Yücel, Y.H., Zhang, Q., Gupta, N., Kaufman, P.L., & Weinreb, R.N. Loss of neurons in magnocellular and parvocellular layers of the lateral geniculate nucleus in Glaucoma. *Arch. Ophthalmol.* **118** (3), 378-384 (2000).

12. von dem Hagen, E.A., Hoffman, M.B., & Morland, A.B. Identifying human albinism: a comparison of VEP and fMRI. *Invest. Ophthalmol. Vis. Sci.* **49** (1), 238-249 (2008).
13. Burkhalter, A., & Bernardo, K.L. Organization of cortico-cortical connections in human visual cortex. *Proc. Natl. Acad. Sci. USA.* **86** (3), 1071-1075 (1989).
14. Mufson, E.J., Brady, D.R., & Kordower, J.H. Tracing neuronal connections in postmortem human hippocampal complex with the carbocyanine Dye DiI. *Neurobiol. Aging.* **11** (6), 649-653 (1990).
15. Wedeen, V.J. *et al.* Diffusion spectrum magnetic resonance imaging (DSI) tractography of crossing fibers. *Neuroimage.* **41** (4), 1267-1277 (2008).
16. Smith, S.M. *et al.* Tract-based spatial statistics: voxelwise analysis of multi-subject diffusion data. *NeuroImage.* **31** (4), 1487-1505 (2006).
17. Newcombe, V.F., Das, T., & Cross, J.J. Diffusion imaging in neurological disease. *J. Neurol.* **260** (1), 335-342 (2013).
18. Behrens, T.E.J. *et al.* Non-invasive mapping of connections between human thalamus and cortex using diffusion imaging. *Nat. Neurosci.* **6** (7), 750-757 (2003).
19. Bassi, L. *et al.* Probabilistic diffusion tractography of the optic radiations and visual function in preterm infants at term equivalent age. *Brain.* **131** (2), 573-582 (2008).
20. Hofer, S., Karaus, A., Frahm, J. Reconstruction and dissection of the entire human visual pathway using diffusion tensor MRI. *Front Neuroanat.* **4**, 1-7 (2010).
21. Fujita, N. *et al.* Lateral Geniculate Nucleus: Anatomic and Functional Identification by Use of MR Imaging. *Am. J. Neuroradiol.* **22** (9), 1719-1726 (2001).
22. McKetton, L., Joy, W., Viviano, J.D., Yücel, Y.H., Gupta, N., & Schneider, K.A. High resolution structural magnetic resonance imaging of the human subcortex in vivo and postmortem. *J. Vis. Exp.* (2015).
23. Fischl, B. FreeSurfer. *NeuroImage.* **62** (2), 774-781 (2012).
24. Yeh, F.C., Verstynen, T.D., Wang, Y., Fernández-Miranda, J.C., & Tseng, W.Y. Deterministic Diffusion Fiber Tracking Improved by Quantitative Anisotropy. *PLoS One.* **8** (11), 807-813 (2013).
25. Jiang, H., van Zijl, P.C., Kim, J., Pearlson, G.D., & Mori, S. DtiStudio: resource program for diffusion tensor computation and fiber bundle tracking. *Comput. Methods. Programs. Biomed.* **81** (2), 106-116 (2006).
26. Smith, S.M. *et al.* Advances in functional and structural MR image analysis and implementation as FSL. *NeuroImage.* **23** (1), 208-219 (2004).
27. Galantucci, S. *et al.* White matter damage in primary progressive aphasias: a diffusion tensor tractography study. *J. Neurol.* **134**, 3011-3029 (2011).
28. Cabin, R.J., &Mitchell, R.J. To Bonferroni or not to Bonferroni: when and how are the questions. *Bull. Ecol. Soc. Am.* **81** (3), 246-248 (2000).
29. Kaiser, P.K. Prospective evaluation of visual acuity assessment: a comparison of snellen versus ETDRS charts in clinical practice (An AOS Thesis). *Trans. Am. Ophthalmol. Soc.* **107**, 311-324 (2009).
30. Farahibozorg, S., Hashemi-Golpayegani, S.M., & Ashburner, J. Age and sex-related variations in the brain white matter fractal dimension throughout adulthood: An MRI study. *Clin. Neuroradiol.* **25** (1), 19-32 (2014).
31. Tian, L., Wang, J., Yan, C., & He, Y. Hemisphere and gender-related differences in small world brain networks: a resting state functional MRI study. *NeuroImage.* **54** (1), 191-202 (2011).
32. Ge, Y., Grossman, R.I., Babb, J.S., Rabin, M.L., Mannon, L.J, & Kolson, D.L. Age-related total gray matter and white matter changes in normal adult brain. Part 1: volumetric MR imaging analysis. *Am. J. Neuroradiol.* **23** (8), 1327-1333 (2002).
33. Zhang, L., Dean, D., Liu, J.Z., Sahgal, V., Wang, X., & Yue, G.H. Quantifying degeneration of white matter in normal aging using fractal dimension. *Neurobiol. Aging.* **28** (10), 1543-1555 (2007).
34. Jones, D.K., Knosche, T.R., & Turner, R. White matter integrity, fiber count, and other fallacies: The do's and don'ts of diffusion MRI. *NeuroImage.* **73**, 239-254 (2013).
35. Coenen, V.A., Huber, K.K, Krings, T., Weidemann, J., Gilsbach, J.M., & Rohde, V. Diffusion-weighted imaging-guided resection of intracerebral lesions involving the optic radiation. *Neurosurg. Rev.* **28** (3), 188-195 (2005).
36. Andrews, T.J. Halperm, SD, Purves, D. Correlated size variations in human visual cortex, lateral geniculate nucleus, and optic tract. *J. Neurosci.* **17** (8), 2859-2865 (1997).
37. Bridge, H., Thomas, O., Jbabdi, S., & Cowey, A. Changes in connectivity after visual cortical brain damage underlie altered visual function. *Brain.* **131**, 1433-1444 (2008).
38. Asman, A.J., Landman, B.A. Non-local statistical label fusion for multi-atlas segmentation. *Med. Image. Anal.* **17** (2), 194-208 (2013).